Photoionization of ultracold and Bose-Einstein-condensed Rb atoms

D. Ciampini, M. Anderlini, J. H. Müller, F. Fuso, O. Morsch, J. W. Thomsen,* and E. Arimondo
INFM, Dipartimento di Fisica E. Fermi, Università di Pisa, Via Buonarroti 2, I-56127 Pisa, Italy
(Received 29 May 2002; published 10 October 2002)

Photoionization of a cold atomic sample offers intriguing possibilities for observing collective effects at extremely low temperatures. Irradiation of a rubidium condensate and of cold rubidium atoms within a magneto-optical trap (MOT) with laser pulses ionizing through one-photon and two-photon absorption processes was performed. Losses and modifications in the density profile of the remaining trapped cold cloud or the remaining condensate sample were examined as functions of the ionizing laser parameters. Ionization cross sections were measured for atoms in a MOT, while in magnetic traps losses larger than those expected for ionization process were measured.

DOI: 10.1103/PhysRevA.66.043409 PACS number(s): 32.80.Pj, 32.80.Rm, 03.75.Fi

I. INTRODUCTION

The recent development of laser cooling and trapping techniques has made possible the controlled realization of dense and cold atomic samples, thus opening the way for spectroscopic investigations in the low and ultralow temperature regimes not accessible with conventional techniques. Cold atoms in magneto-optical traps (MOT's) have been used as excellent tools for the measurement of ionization cross sections. In particular for alkali-metal atoms [1–8] and for magnesium [9] valuable data have been obtained using the trap population dynamics as a sensitive monitor of the trap loss induced by the ionizing radiation, extracting wavelength dependencies and absolute values for the cross sections. More recently, ultracold plasmas have been created making use of laser cooled atomic samples and laser excitation to high Rydberg states [10]. To understand the relaxation of such a system toward equilibrium many phenomena such as recombination and superelastic collisions in a completely different temperature regime for plasmas have to be taken into account. Moreover, a frozen Rydberg gas can be created with intriguing transport properties, like quasimetallic behavior or delayed electron emission [11]. In these systems the collective character of the dynamics is due to the strong interaction between charged and highly excited particles.

The realization of Bose-Einstein condensates (BEC's) of alkali-metal atom vapors has attracted much interest to aspects of photon-matter interaction arising from the coherent nature of the atomic ensemble. Recently, attention has been paid to the analysis of photoionization of a BEC by monochromatic laser light [12]. The products of the photoionization process (electrons and ions) obey Fermi-Dirac statistics. Owing to the coherent nature of the initial atomic ensemble and the narrow spectral width of the laser ionization source, the occupation number of the electron/ion final states can approach unity, especially for excitation close to threshold. In this regime the ionization rate should be reduced by the Pauli blockade and determined by a balance between the laser light acting on the atoms and the rate of escape of the ionization products from the condensed system.

When photoionizing cold atoms, at decreasing temperature and at increasing atomic density, the interaction between the charged particles and the neutral ''dielectric'' background can become significant. Additional information about the energy transfer from the charged species to the neutral particles can be obtained using nondissipative traps, such as magnetic traps, and using the atom dynamics as a monitor. An ion localized inside a condensate modifies the density distribution of the condensate dielectric background by attracting the atoms toward itself. The classical interaction energy between a single ion and a polarized ground state condensate at a distance typical for a condensate density of 10^{14} cm^{-3} is larger than typical chemical potentials in Bose-Einstein condensates (h times 100 Hz). This means that locally the polarization effect is important for the condensate dynamics and may even lead to destruction of the condensate phase. As a consequence, the observable effect depends on the interaction time between ions and condensate: apart from the recoil picked up from the ionizing photon, in real experiments stray electric fields might limit this interaction time. Examining the condensate cloud remaining after the laser excitation, the atom-ion/electron interaction for weakly ionized clouds may show significant changes of the density and momentum distribution [13]. Furthermore, the interaction of the charged particles among themselves will play an important role for higher fractions of ionized particles, with plasma formation and collective effects.

In this paper we report, and compare, the results of an experimental investigation of the photoionization process within a rubidium condensate and within the cold rubidium sample of a MOT. The condensate photoionization process originates from the ground state, while for the MOT sample results from both the ground and the first excited electronic states have been obtained. We investigated ionization by means of one-photon and two-photon single color processes using various pulsed and cw laser sources, more precisely 296 nm for one-photon ionization and 580–600 nm for two-photon ionization from the $5S_{1/2}$ ground state, and 296 and 421 nm radiation for one-photon ionization from the $5P_{3/2}$ state. The ionization process was examined through the losses from the sample, a cold cloud inside a MOT or a

*Permanent address: Niels Bohr Institute, Oersted Laboratory, University of Copenhagen, DK-2100 Copenhagen, Denmark.

 ©2002 The American Physical Society

magnetic trap, or a condensate inside a magnetic trap. Our approach is based on trap loss ionization spectroscopy with the photoionization losses measured as an additional decay after the trap loading.

Section II recalls briefly the model for photoionization induced trap loss, concentrating on the use of a pulsed laser. Section III describes the experimental setup and the characteristics of the applied pulsed and cw laser radiation. Section IV analyzes and discusses the experimental results obtained on the thermal and condensate cloud, separating the MOT and magnetic trap experiments. Section V concludes the present investigation.

II. TRAP LOSS SPECTROSCOPY

A. Photoionization

The dynamics of the number N of trapped atoms in a MOT in the constant density regime and with the trap loading shut off predicts an exponential decay, with a time constant $1/\gamma$, determined by collisions with the background gas and intratrap collisions. In the presence of ionization by a cw laser, additional losses with rate $\gamma_{\rm ph}$ shorten the lifetime of the trap and the equation of evolution for N becomes [1]

$$\frac{dN}{dt} = -\gamma N - \gamma_{\rm ph} N. \tag{1}$$

Hence, if N_0 is the initial number of atoms,

$$N(t) = N_0 e^{-(\gamma+\gamma_{\rm ph})t}. \tag{2}$$

When using photons above the ground state ionization threshold on a MOT, the loss rate $\gamma_{\rm ph}$ contains the contributions from the $5S$ rubidium ground state ionization rate R_{5S} and from the $5P$ rubidium excited state ionization rate R_{5P}:

$$\gamma_{ph} = (1-f)\mathsf{R}_{5S} + f\mathsf{R}_{5P}, \tag{3}$$

with f the fraction of atoms in the excited state. That fraction f, under standard MOT operating conditions, can be calculated from the MOT laser parameters as in Refs. [2,4]. For a cold cloud in a magnetic trap or for a condensate, Eq. (1) can also be applied. In that case the excited state fraction f is equal to zero, so that the ionization loss depends on the ground state rate R_{5S} only.

In the case of one-photon ionization by a laser with a photon flux $F_{\rm ph}$, the ionization rate is

$$\mathsf{R}_{5l} = \sigma_{5l}^{(1)} \beta^{(1)} F_{\rm ph}, \tag{4}$$

with $l=(S,P)$, $\sigma_{5l}^{(1)}$ being the one-photon ionization cross-section and $\beta^{(1)}$ a geometrical correction coefficient. For a two-photon ionization process with cross section $\sigma_{5l}^{(2)}$ and geometrical correction coefficient $\beta^{(2)}$, the ionization rate is

$$\mathsf{R}_{5l} = \sigma_{5l}^{(2)} \beta^{(2)} (F_{\rm ph})^2. \tag{5}$$

The geometrical coefficients $\beta^{(k)}$ take into account the spatial distribution of the laser beam and the atomic sample. For a Gaussian laser beam with waists w_x and w_y centered on a Gaussian atomic distribution with sizes L_x and L_y, and assuming the density distribution of the target atoms not depleted by the laser, the geometrical corrections are

$$\beta^{(k)} = \frac{1}{\sqrt{[1+k(L_x/w_x)^2][1+k(L_y/w_y)^2]}}, \tag{6}$$

with $k=(1,2)$. The correction approaches unity for laser beam sizes larger than the atomic sample size. The ionization photon flux $F_{\rm ph}$ is connected to the photon number $n_{\rm ph}$ and area $A_{\rm ph}=\pi w_x w_y/2$, or to the intensity $I_{\rm ph}$ and wavelength $\lambda_{\rm ph}$, by

$$F_{\rm ph} = \frac{n_{\rm ph}}{A_{\rm ph}} = \frac{I_{\rm ph}\lambda_{\rm ph}}{hc}. \tag{7}$$

For the ionization by a pulsed laser with pulse duration $\tau_{\rm ph}$, the ionization probability is

$$P_{\rm ph} = \gamma_{\rm ph}\tau_{\rm ph}. \tag{8}$$

In analogy with Eq. (2), the atom number left in the trap (either magneto-optical or magnetic) after the application of a single laser pulse is

$$N_{\rm ph} = N_0(1-P_{\rm ph}) = N_0(1-\gamma_{\rm ph}\tau_{\rm ph}). \tag{9}$$

For a sequence of laser pulses, we suppose that each ionization process is not modified by the previous photoionization history. Thus the application of a sequence of m pulses leads to the following remaining number:

$$N_{\rm ph} = N_0(1-\gamma_{\rm ph}\tau_{\rm ph})^m. \tag{10}$$

If we apply a pulse sequence with rate $r_{\rm ph}$, at the time t the atom number becomes

$$N(t) = N_0 e^{-\gamma t}(1-\gamma_{\rm ph}\tau_{\rm ph})^{r_{\rm ph}t}. \tag{11}$$

In the case of a small ionization probability, the decrease in the atom number is well approximated by an exponential decay, as in Eq. (2) for the cw laser, with an effective ionization decay $\gamma_{\rm ph}^{\rm eff}$,

$$\gamma_{\rm ph}^{\rm eff} = \gamma_{\rm ph}\tau_{\rm ph} r_{\rm ph} = [(1-f)\mathsf{R}_{5S} + f\mathsf{R}_{5P}]\tau_{\rm ph} r_{\rm ph}. \tag{12}$$

We verified Eq. (11) to be valid by changing the repetition rate $r_{\rm ph}$, and hence the time separation between successive pulses, and obtaining consistent results for $\gamma_{\rm ph}^{\rm eff}$.

B. Scattering and dipole force

Apart from changing the internal atomic state, the ionizing laser radiation also acts on the center-of-mass motion of the atoms through the scattering and dipole forces (see, e.g., [15] for an overview and [16] for the case of pulsed radiation). For ionization above threshold the excess energy of the photon is converted into kinetic energy of the fragments, imparting large momentum to the electron and ion. For trap loss spectroscopy only the radiation forces acting on the atoms remaining in bound states within the trap need to be

considered for additional loss mechanisms. The dissipative environment of a MOT with a typical effective trap depth of 300 mK safely recaptures and cools atoms with velocities of some 10 m/s, while in a conservative magnetic trap with typical depth of 50 μK atoms accelerated to 10 cm/s can escape from the trap.

The relative roles of the scattering and dipole forces acting on the atoms depend mainly on the laser detuning from the atomic transitions. For most of our investigations with pulsed lasers, the laser detuning was so large that the scattering forces could be neglected. For the case of a condensate there is a subtle difference between the effects of the scattering and dipole forces. In a spontaneous emission event the photon recoil is picked up by this atom, as long as the condensate sound velocity is smaller than the atomic recoil velocity. Instead, the dipole force due to the coherent redistribution of laser photons acts on the whole condensate cloud. For a constant intensity gradient over the condensate, the center-of-mass motion of the condensate will be driven by the dipole force without internal excitation. By contrast, for laser beam sizes comparable to the condensate size, the gradient of dipole force produces also internal excitations of the condensate. For the impulse approximation in the case of pulsed radiation, a complicated phase pattern is imprinted onto the condensate cloud, which subsequently evolves into considerable modifications of the condensate density distribution, catalyzing the formation of solitons, as in Ref. [17], or splitting the condensate cloud into pieces. Part of these fragments may acquire a high enough kinetic energy to leave the magnetic trap potential, hence leading to additional trap losses. Rather than attempting to model the complicated cloud dynamics, in Sect. IV B we will only estimate the kinetic energy imparted by the laser pulse to a single atom.

C. Collisions

Additional trap losses may be caused by inelastic collisions between the ionization products, electrons and ions, and the thermal or condensed cloud remaining in the trap. We have found very little information available for those very low energy collisional processes. Using the cross section for collisions of 10 meV electrons with carbon dioxide molecules [18] or the scattering length for the electron-Rb collisions reported in Ref. [19], we estimated the collisional processes to produce negligible additional trap losses. We should also consider that, after the ionization, a recombination process produces atoms in highly excited Rydberg states, and those atoms will thermalize within the condensate. During this process, inelastic collisions can lead to additional losses, whose contribution we cannot easily estimate.

III. EXPERIMENTAL SETUP

Our experimental apparatus, described in Ref. [20], was based on a double MOT system, divided into a high vacuum region optimized for collecting Rb atoms in a MOT, and a second region of low background pressure, into which the atoms were collected for transfer to the high vacuum MOT. Photoionization investigations were performed in the high vacuum MOT. For the experimental parameters of our MOT lasers (intensity $I=16.5$ mW/cm^2, detuning $\delta=-2.2\Gamma$) we derived an excited state fraction $f=0.14\pm0.02$.

The atoms from the high vacuum MOT can be transferred into a magnetic trap, in our case a triaxial time-orbiting potential trap (TOP). Compressing the trapped cloud and applying forced evaporative cooling with rf induced spin flips, the BEC phase transition was reached with typically 5×10^4 atoms. "Pure" $|F=2,\ m_F=2\rangle$ condensates contained up to 2×10^4 atoms in an ellipsoid whose average dimension was in the 5 μm range. Instead, the dimension of the noncondensed cloud inside the TOP was in the 40-100 μm range. Depending on the chosen sequence of cooling and trapping steps, noncondensed or condensed samples with temperatures ranging from a few hundreds of microkelvins down to tens of nanokelvins with atomic densities of 10^{10}–10^{14} atoms/cm^3 were prepared.

The present experimental setup does not include a charge detector to monitor directly the production of positive and negative charges. Thus the action of the photoionizing laser was monitored through the decrease of the atoms remaining in the trap, applying a shadow imaging detection using a 780 nm near-resonant probe laser beam. The absorptive shadow cast by the cold atoms was imaged onto a charge-coupled device camera. Measurements on both condensates and very cold thermal clouds were performed after a few milliseconds of free fall of the released atomic clouds, when their typical dimensions were of the order of 30–300 μm. The atomic samples remaining after the photoionization process contained a number of atoms large enough to measure their temperature and density distributions. Within the magnetic trap both a sample of thermal atoms with about 10^6 rubidium atoms cooled by evaporative cooling down to $T=400$ nK and a condensate were photoionized.

The 4.177 eV energy threshold for ionization of rubidium atoms from the $5S_{1/2}$ ground state can be reached by a single photon of 296.815 nm wavelength. Alternatively, the ionization threshold can be crossed using two photons aroud 594 nm, with a substantially larger radiation intensity needed since there is no resonant intermediate level for the two-photon process. We irradiated the cold atom with pulsed lasers operating around 594 nm and 296 nm, and with a cw laser at 421 nm.

The 580–600 nm radiation was produced by an excimer-pumped dye laser, with intensities in the hundreds of MW/cm^2 range and a laser pulse duration $\tau_{\rm ph}$ of 10 ns. Laser pulse repetition rates $r_{\rm ph}$ up to 12 Hz were used. The excess energy $E_{\rm ex}$ of the ionizing photons, and therefore the kinetic energy of the released electrons, was around 8.5 meV with an energy spread due to the laser linewidth of around 0.1 meV. The 296 nm radiation was generated from the yellow radiation by frequency doubling within a beta barium borate (BBO) crystal, with 15% efficiency. The wavelength used corresponded to an electron excess energy $E_{\rm ex}$ of 10.4 ±0.1 meV. The 594 nm dye laser radiation was focused down to 80 μm on the rubidium atoms, while for the 296 nm radiation, owing to beam astigmatism, beam waists of 0.36 $\times1.6$ mm for the MOT and 0.16×0.78mm for the TOP were achieved.

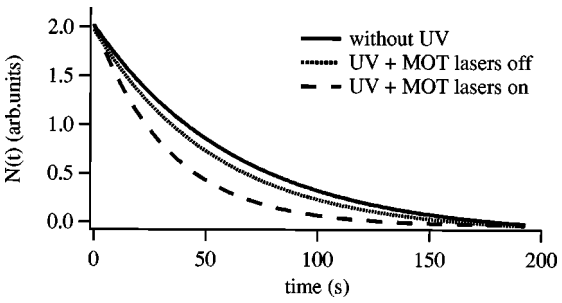

FIG. 1. Time decay for the fluorescence from the rubidium atom MOT in the absence (continuous line) and in the presence of 296 nm uv light (dashed and dotted lines). For the case of the dotted line the MOT lasers were switched off before applying the uv light in order to populate the $5S_{1/2}$ ground state only. A $r_{\rm ph}=10$ Hz pulse repetition rate was used, with 130 μJ pulse energy.

For the 421 nm radiation a grating stabilized diode laser operating at 842 nm injected a tapered amplifier delivering power in excess of 500 mW. The ir radiation was frequency doubled using a lithium triborate (LBO) crystal placed inside an external enhancement resonator [21]. Around 10 mW of narrowband cw radiation at 421 nm were available. The 421 nm wavelength was chosen in order to use the $6P_{1/2}$ or $6P_{3/2}$ level as a near-resonant intermediate step for a two-photon process from the ground state leading to an electron excess energy of 1.7 eV. When applied to atoms stored in a MOT, the one-photon process out of the populated $5P_{3/2}$ state is dominant, releasing electrons with an excess energy of 0.34 eV.

IV. PHOTOIONIZATION RESULTS

A. MOT

The frequency doubled radiation 296 nm pulsed laser induced single-photon ionization of the ground state and first excited state. The MOT atoms were by illuminated a photon flux $F_{\rm ph}=2\times10^{24}$ cm^{-2} s^{-1}. Decay profiles of the 780 nm wavelength MOT fluorescence, proportional to the trapped atom number, after shutting off the loading are displayed in Fig. 1. To separate in Eq. (12) the contributions due to the ionization from the ground $5S_{1/2}$ and excited $5P_{3/2}$ states, we combined fast switching of the MOT laser beams with the timing of the ionization pulses. The solid line in Fig. 1 shows the exponential decay in the absence of uv photoionization light, with a decay time $\gamma^{-1}=60$ s. The dashed and dotted lines correspond to the application of the pulsed uv light to a cw and a synchronously switched MOT, respectively. In the synchronous operation mode the MOT lasers were switched off for 60 μs, leaving ample time for the atoms to decay back to the ground state before interacting with the uv pulse while keeping negligible the ballistic expansion of the cloud. Using the fraction of excited atoms *f*, we derived from $\gamma_{\rm ph}$ (around one-fifth of γ) the following values of the photoionization cross sections:

$$\sigma^{(1)}_{5S_{1/2}}=(0.76\pm0.15)\times10^{-19}\ \text{cm}^2, \tag{13a}$$

$$\sigma^{(1)}_{5P_{3/2}}=(5.4\pm1.2)\times10^{-18}\ \text{cm}^2. \tag{13b}$$

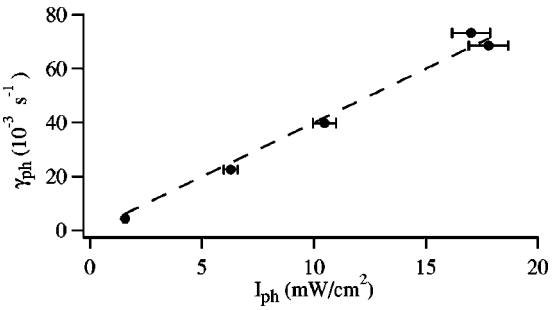

FIG. 2. Additional loss rate $\gamma_{\rm ph}$ introduced in the MOT evolution by the presence of the 421 nm cw laser, as a function of the laser intensity $I_{\rm ph}$. From these data the photoionization cross section for the excited $5P_{3/2}$ state was derived.

The ground state ionization cross-section value is in reasonable agreement with the value measured in the late 1960's by Marr and Creek [22] using the absorption of uv light emitted from a discharge lamp by hot Rb vapors, and later derived theoretically in Refs. [23,24]. Since we used interleaved scans for these measurements, our largest systematic error source, the intensity determination of the ionizing laser, drops out for the ratio of the two cross sections

$$\frac{\sigma_{5P_{3/2}}}{\sigma_{5S_{1/2}}}=71\pm10, \tag{14}$$

the error being given only by the uncertainty in *f*.

In the ground state two-photon ionization by the yellow 594 nm pulsed laser with photon flux $F_{\rm ph}\simeq10^{27}$ cm^{-2} s^{-1}, we also examined the decay of the MOT fluorescence emission. Using the method of interleaved cw and synchronously switched runs described above, we also verified that the two-photon ionization contribution from the excited $5P_{3/2}$ state could be neglected in this case. The additional measured loss rate introduced by the pulsed dye laser with rate $r=11$ Hz was $\gamma^{\rm eff}_{\rm ph}=1.14\times10^{-3}$ s^{-1}. Using Eq. (12) the ionization probability $P_{\rm ph}$ by a single pulse is 1×10^{-4}, corresponding to a two-photon ionization cross section from the ground state

$$\sigma^{(2)}_{5S_{1/2}}=(11\pm6)\times10^{-49}\ \text{cm}^4\,\text{s}. \tag{15}$$

This value agrees quite well with the theoretical prediction 5×10^{-49} cm^4 s, calculated by Bebb [25].

Using the 421 nm cw laser, we studied the decay of the MOT population due to ionization from the first excited state, whose cross section was estimated by Aymar *et al.* [23]. For the two-photon ionization from the ground state the cross section $\sigma^{(2)}_{5S}=4\times10^{-49}$ cm^4 s estimated in [25] predicts a negligible ground state ionization with the available photon flux. The measured additional MOT loss rates $\gamma_{\rm ph}$ are plotted in Fig. 2 as a function of the photoionizing laser intensity $I_{\rm ph}$. From these data we obtained the following value for the photoionization cross section at $\lambda_{\rm ph}=421.66$ nm:

$$\sigma^{(1)}_{5P_{3/2}}=(1.34\pm0.16)\times10^{-17}\ \text{cm}^2. \tag{16}$$

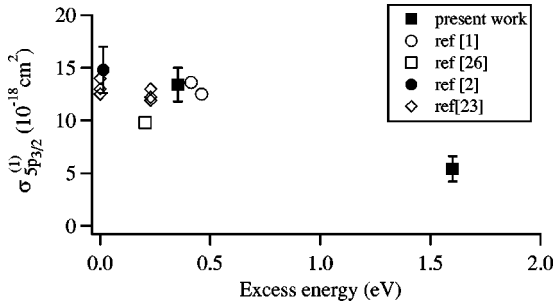

FIG. 3. One-photon ionization cross sections in the Rb MOT from the excited state $5P_{3/2}$ as a function of the electron excess energy. The filled squares are our experimental results for $\lambda_{ph}=296$ nm and $\lambda_{ph}=421$ nm. Other data points are extracted from the literature.

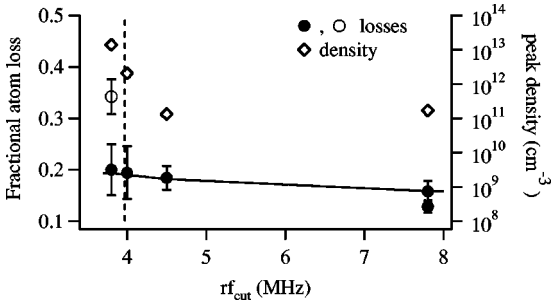

FIG. 4. Fractional loss of atoms after exposure to 120 pulses of the 296 nm laser inside the magnetic trap (filled circles) as a function of the final frequency for rf evaporation (for the open circle data point a longer time of flight was used). The decreasing rf cut produced an increasing atomic peak density (open diamonds). The dashed line indicates the condensation threshold position. The continuous line models the effect of the changing size of the cloud within the spatial distribution of the uv beam.

Figure 3 shows the measured data for the photoionization cross section from the rubidium excited state $5P_{3/2}$ for various wavelengths of the ionizing laser. Our experimental points at 296 nm (pulsed) and 421 nm (cw) are in good agreement with the values previously measured by Dinneen *et al.* [1], Gabbanini *et al.* [2], and Klyucharev and Sepman [26], the last one for an unresolved fine structure $5P$ state, and the two theoretical estimates of Aymar *et al.* [23]. Within the explored range the cross-section dependence on E_{ex} is fitted by a straight line, while at larger excess energy an $E_{ex}^{-9/2}$ dependence is expected [23].

B. Magnetically trapped atoms

In the ionization experiment performed with uv light at 296 nm a lower peak intensity (70 μJ) and the large beam size led to a single-pulse ionization probability of 0.002. Because a single-pulse produced a loss of atoms too small to be directly detected, we illuminated the magnetically trapped atoms (condensate and noncondensate) with a sequence of 120 pulses, at a repetition rate of 11 Hz. We performed the investigation of the ionization losses starting with an initial cold cloud of 10^6 atoms and, varying the final rf frequency cut, we ionized clouds with decreasing temperature and increasing atom density. Finally, for radio-frequency cuts below the 3.95 MHz threshold, we ionized a pure condensate. Data for the peak density and the fractional atom loss are reported in Fig. 4 as a function of the final rf value. The measured total fractional losses between 15% and 20% were compared to the single-pulse loss extracted from the MOT measurements described by the continuous curve in Fig. 4, taking into account the changing size of the atomic cloud via the geometric factor $\beta^{(1)}$ of Eq. (4) and including an overall scale factor of 1.5, due to an estimated misalignment of 100 μm between the atomic cloud and the laser beam. We verified that the temperatures of the thermal clouds were unaffected by the laser pulses within the experimental uncertainty of 5%. However, when using a longer time of flight before imaging for a pure Bose-condensed cloud (in order to decrease the optical density, thus getting more reliable data for the number of atoms), we measured higher losses (the open circle in Fig. 4). This result indicates the presence of very low energy thermal atoms removed from the condensate but still trapped, albeit with a spatial density below our detection noise. Thus the 296 nm laser acting on a condensate produces additional loss of low energy thermal atoms ejected from the condensate cloud. Since for the large beam size and the moderate pulse energy we did not expect a significant contribution of scattering and dipole forces, we have taken these additional losses as evidence for the interaction of ionization products with the condensate background.

Using the 594 nm pulsed radiation, we irradiated the magnetically trapped atoms either with few pulses or by applying a single laser pulse. The puzzling result of these investigations was the measurement of a large loss rate, larger by a factor of 10 than the value expected from the previously measured two-photon ionization cross section. Moreover, the measured trap losses depended strongly on the alignment of the photoionizing laser with respect to the magnetic trap. For perfect alignment and small clouds we expected an ionized fraction of 2%, while losses of 20% were observed. An example of the measured fractional loss of atoms from the magnetic trap, normalized to the laser pulse energy, is reported in Fig. 5 as a function of the wavelength of the ionizing laser. The data of Fig. 5 do not exhibit clear evidence of the threshold behavior expected for a two-photon ionization process. These results suggest the presence of other loss

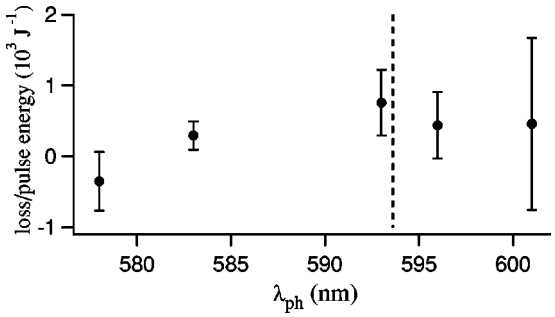

FIG. 5. Loss rate for a single laser pulse, normalized by the pulse energy, as a function of the dye laser wavelength. The vertical line indicates the threshold wavelength for the two-photon ionization from the ground state.

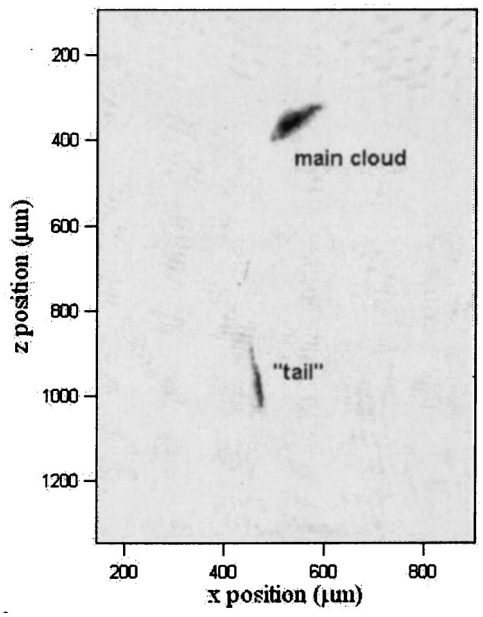

FIG. 6. Shadow image of a condensate after the application of a single dye laser pulse at 594 nm. The condensate is deformed and a secondary condensate containing around 30% of the original atoms is present (the periodic circular fringe patterns are an artifact of the imaging technique). The size of the main cloud at the ionization time was 7 μm, and the trapping frequency 23 Hz, and the time of flight 18 ms.

mechanisms masking the ionizing process. In a magnetic trap, in fact, every process changing the hyperfine or *m* sublevel leads to atom loss.

The presence of more complex trap loss processes is indicated also by the spatial distribution of the atoms inside the magnetic trap after the application of a single laser pulse at 594 nm. For both the condensate and the thermal cloud of magnetically trapped atoms, we noticed that the laser pulse ejected a secondary cloud, a ''tail,'' from the original one, as shown in Fig. 6. The shadow image of Fig. 6, obtained after 11 ms of evolution of the condensates within the magnetic trap, shows two clouds, the upper cloud at the place of the original one and the ejected secondary cloud separated spatially, at a lower vertical position. The secondary cloud of Fig. 6 contained around 30% of the total number of atoms, but in other conditions the secondary cloud contained a fraction reaching 50%. Measuring the atomic density and temperature for the two clouds separately, we derived that the phase space density of the ejected cloud was comparable to the remaining fraction of the original cloud. Below the condensation threshold both remaining clouds had a phase space density far above 1. This suggests that the laser pulse split the original condensate into two condensed clouds. Both of the observed clouds were strongly deformed with respect to the unperturbed condensate, showing a close to spherical density distribution after the same time of flight. The aspect ratio and orientation of the deformed cloud depended on the evolution time within the magnetic trap after the laser excitation. Moreover a detailed analysis, outlined below, showed for the main cloud a negligible center-of-mass motion, while

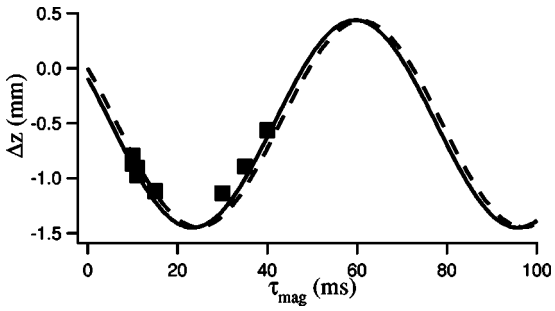

FIG. 7. Data for the relative displacement Δz of the $|F=2, m_F=1\rangle$ secondary condensate, ejected from the $|F=2, m_F=2\rangle$ primary one after a single 594 nm laser ionization pulse, versus the evolution time τ_{magn} within the magnetic trap. The oscillating fit functions correspond to different initial velocities $v_z(0)$ of the secondary cloud, $v_z(0)=0$ for the dashed line and $v_z(0)=-0.5$ cm/s for the continuous line, whose vertical shift for $\tau_{\mathrm{magn}}=0$ is due to free fall evolution of the condensate during the time of flight.

the secondary cloud acquired a center-of-mass motion during the interaction with the laser pulse.

In order to understand the nature of the secondary cloud, we used the magnetic trap as a Stern-Gerlach analyzer. We measured the position of the secondary condensate as a function of the evolution time τ_{magn} within the magnetic trap after the application of the laser pulse, with results shown in Fig. 7. From the oscillatory behavior of the difference in position of the center of mass for the two clouds we inferred that the secondary cloud consisted of rubidium atoms in the $|F=2, m_F=1\rangle$ Zeeman state, excluding the $|F=1, m_F=-1\rangle$ state with similar magnetic moment, because our detection was sensitive only to atoms in the $F=2$ state [27]. Owing to the different magnetic moment of this state, both the frequency of the harmonic sloshing motion and the equilibrium position differ from those for atoms in the $|F=2, m_F=2\rangle$ state. A fit to the measured position data, assuming that the secondary cloud was created at the instant of the laser pulse from the position of the mother condensate, revealed that the secondary cloud started its oscillation with an initial velocity $v_z(0)=(-0.5\pm0.2)$ cm/s, i.e., a velocity pointing downward along the vertical axis [28]. The laser pulse propagated at an angle of about 35° with respect to the horizontal *x*-*y* plane and pointed downward in the *z*-*y* plane, while the laser light was polarized along the *x* direction of Fig. 6. The atoms are polarized along the direction of the bias field, rotating in the horizontal *x*-*y* plane with frequency 10 kHz. Changing the timing of the laser pulse with respect to the bias field rotation, we found no qualitative difference in the atomic response for parallel and crossed electric and magnetic fields.

To judge how the direct mechanical effect of the laser pulse could be responsible for the observed complex behavior of the clouds and of the anomalously high losses, we estimated the role of the dipole forces in a single-atom picture. Placing a rubidium atom at the steepest slope of the spatial laser beam profile during the pulse, we estimated an atom to acquire a velocity of 0.8 cm/s under application of the 594 nm pulse. Based on this estimate the atomic kinetic

energy of 40 μK would be well below the trap depth, and direct losses due to the dipole force would not be expected. An additional puzzle is associated with the transfer of atoms from the initial $m_F=2$ state to the $m_F=1$ final one. Such a transfer could be created by a Raman process associated with the absorption and emission of the laser photons, with a probability enhanced by the atomic stimulated emission as in atom laser emission. However, Raman transfer between Zeeman sublevels is forbidden by the $\Delta m_F=0$ selection rule for the interaction with a linearly polarized laser field. A violation of the selection rule may arise because the trap magnetic field is not constant during the laser pulse or by fluctuations of the laser polarization on the time scale of a single pulse. Notice that Raman scattering processes do not produce losses in a MOT, where every Zeeman sublevel of the ground state is trapped and the kinetic energy acquired is smaller than the trap depth. As mentioned above, the shape of the detected clouds was grossly different from the shape of unperturbed condensates. Such a shape deformation could be associated with the asymmetry in electron emission produced by the photoionization process, exciting complicated oscillations in the original and secondary condensate clouds.

Finally, we excited thermal clouds and condensates with the 421 nm radiation detuned by 12 GHz above the resonance and focused to 30 μm$\times$3.3 μm. At such a detuning the scattering force still dominates the atomic losses from the magnetic trap, and the trap losses due to the two-photon ionization from the ground state could not be directly measured. We observed that the condensate cloud falling under gravity through the 421 nm laser beam was split into two condensate clouds, the reflected and transmitted, respectively, again without measurable additional atomic losses. Note that in this case the interaction time with the laser radiation is orders of magnitude longer than for pulsed lasers, so that a complicated dynamics may be produced.

V. CONCLUSIONS

We applied trap loss spectroscopy to measure the photoionization cross sections of rubidium atoms confined in a MOT, making use of cw and pulsed laser. We verified that the use of pulsed lasers did not limit the accuracy reached in the cross-section determination. We demonstrated that the photoionization of magnetically trapped thermal and condensed atoms instead does not represent a precise tool for cross-section determination. In effect the magnetic trap depth is smaller than the MOT depth, and the laser action on the cold atomic cloud may produce additional processes leading to atomic losses from the trap, masking the ionization losses. We have observed that both scattering and dipole forces associated with strong pulsed lasers may impart a kinetic energy large enough to overcome the trap depth. Moreover, dealing with a condensate cloud, additional losses appear that are probably due to the creation of a dilute thermal cloud.

We have discovered that the application of intense pulsed radiation leads to huge excitation and macroscopic splitting of a condensate without compromising its phase space density. We identified the transfer of atoms to the $|F=2, m_F=1\rangle$ level as an important process, but the detailed microscopic mechanism remains unclear and will be the subject of further studies.

On the basis of the photoionization cross sections measured within a MOT we estimated that we created charged clouds and condensates in magnetic traps containing a fraction of 0.2% and 2% of ions at a time for the one-photon and two-photon experiments, respectively. We have not observed any dramatic instability which could be triggered by the strong polarization of those charged condensates. However, we take the higher losses measured following the one-photon ionization of a condensate as an indication of the interaction between the ionization products and the condensate background. Additional processes such as collisions with cold electrons and ultracold neutrals, recombination, and collective processes in the weak and cold plasma could modify the atomic cloud evolution and in part be responsible for the more complicated dynamics observed after the two-photon excitation in the condensate. In future experiments we plan to use cw sources to ionize condensed clouds to disentangle scattering and dipole force effects from the rich and interesting physics of cold charged particles in quantum degenerate clouds.

ACKNOWLEDGMENTS

The authors wish to thank G. Alber, W. M. Fairbank, Jr., C. Fort, P. Gould, M. Inguscio, S. Manson, and P. Zoller for illuminating discussions. This research was supported by the Sezione A of INFM, Italy through a PAIS Project, by the MIUR, Italy through a PRIN Project, and by the EU through Contract No. HPRN-CT-2000-00125.

[1] T.P. Dinneen, C.D. Wallace, K.N. Tan, and P.L. Gould, Opt. Lett. **17**, 1706 (1992).

[2] C. Gabbanini, S. Gozzini, and A. Lucchesini, Opt. Commun. **141**, 25 (1997).

[3] C. Gabbanini, F. Ceccherini, S. Gozzini, and A. Lucchesini, J. Phys. B **31**, 4143 (1998).

[4] O. Maragò, D. Ciampini, F. Fuso, E. Arimondo, C. Gabbanini, and S.T. Manson, Phys. Rev. A **57**, R4110 (1998).

[5] B.M. Patterson, T. Takekoshi, and R.J. Knize, Phys. Rev. A **59**, 2508 (1999).

[6] F. Fuso, D. Ciampini, E. Arimondo, and C. Gabbanini, Opt. Commun. **173**, 223 (2000).

[7] V. Wippel, C. Binder, W. Huber, L. Windholz, M. Allegrini, F. Fuso, and E. Arimondo, Eur. Phys. J. D **17**, 285 (2001).

[8] B.C. Duncan, V. Sanchez-Villicana, P.L. Gould, and H.R. Sadeghpour, Phys. Rev. A **63**, 043411 (2001).

[9] F. Ruschewitz, J. L. Peng, R. Degner, H. Hinderthuer, D. Scheller, D. Bettermann, W. Ertmer, in Proceedings of the 1996 European Quantum Electronics Conference (unpublished), p. 112; D.N. Madsen and J.W. Thomsen, J. Phys. B **35**,

2173 (2002).
[10] T.C. Killian *et al.*, Phys. Rev. Lett. **83**, 4776 (1999); S. Kulin, *et al., ibid.* **85**, 318 (2000); M.P. Robinson, *et al., ibid.* **85**, 4466 (2000); T.C. Killian, *et al., ibid.* **86**, 3759 (2001); S.K. Dutta, *et al., ibid.* **86**, 3993 (2001).
[11] R. Côté, Phys. Rev. Lett. **85**, 5316 (2000).
[12] I.E. Mazets, Quantum Semiclassic. Opt. **10**, 675 (1999).
[13] In the He* condensates of [14] ions were present due to Penning collisions, but the interaction time between ions and neutrals was extremely short due to the high released energy.
[14] A. Robert *et al.*, Science **292**, 461 (2001); F. Pereira Dos Santos *et al.*, Phys. Rev. Lett. **86**, 3459 (2001).
[15] H. J. Metcalf and P. van der Straten, *Laser Cooling and Trapping* (Springer, New York, 1999).
[16] M. Mützel, D. Haubrich, and D. Meschede, Appl. Phys. B: Lasers Opt. **70**, 689 (2000).
[17] S. Burger *et al.*, Phys. Rev. Lett. **83**, 5198 (1999); J. Denschlag *et al.*, Science **285**, 571 (2000).
[18] D. Field, N.C. Jones, S.L. Lunt, and J.-P. Ziesel, Phys. Rev. A **64**, 022708 (2001).
[19] C.H. Greene, A.S. Dickinson, and H.R. Sadeghpour, Phys. Rev. Lett. **85**, 2458 (2000).
[20] J.H. Müller, D. Ciampini, O. Morsch, G. Smirne, M. Fazzi, P. Verkerk, F. Fuso, and E. Arimondo, J. Phys. B **33**, 4095 (2000).
[21] Model TA-SHG-100 by Toptica.
[22] G.V. Marr and D.M. Creek, Proc. R. Soc. London, Ser. A **304**, 233 (1968).
[23] M. Aymar, O. Robaux, and S. Wane, J. Phys. B **17**, 993 (1984).
[24] M.G.J. Fink and W.R. Johnson, Phys. Rev. A **34**, 3754 (1986), and references therein.
[25] H.B. Bebb, Phys. Rev. **149**, 25 (1966).
[26] A.I. Klyucharev and V.Yu. Sepman, Opt. Spectrosc. **38**, 712 (1975).
[27] We confirmed the absence of atoms in the $|F=1\rangle$ hyperfine states by applying a repumper laser before imaging the primary and secondary clouds and verifying that the atom numbers in the clouds were not modified.
[28] We allowed for a 2% accuracy in the magnetic field calibration.